CLM-P853

CLM-P853

Effects of a resistive wall on MHD instabilities

T.C. Hender
C.G. Gimblett
D.C. Robinson

UK ATOMIC ENERGY AUTHORITY

Culham Laboratory

Effects of a resistive wall on MHD instabilities

T.C.Hender C.G.Gimblett D.C.Robinson

Culham Laboratory, Abingdon, OX14 3DB, UK

(Euratom/UKAEA Fusion Association)

Abstract

Linear and non-linear MHD calculations are presented to examine the effect of a finite conductivity (resistive) wall on plasma stability. Near $q_\psi=2$ in the tokamak and generally in the RFP, ideal modes are found, with a growth rate which varies inversely with the wall time constant. Resistive tearing modes can also be destabilised by a finite conductivity wall, but sufficiently fast plasma rotation can in turn stabilise these instabilities. Non-linearly it is shown that the eddy currents driven in the resistive wall, by rotating MHD activity, produce a torque which opposes and slows the plasma rotation. This effect can be particularly strong in the RFP and leads to mode lock times which are shorter than in the tokamak.

1. Introduction

In the majority of magneto-hydrodynamic (MHD) simulations it is assumed that the plasma is surrounded by a perfectly conducting wall. In reality in the tokamak and reverse field pinch (RFP) the wall has a finite conductivity, and a time constant for magnetic field penetration which is less than or comparable with the plasma pulse duration and field diffusion time. In this paper we will examine the effects of a finite conductivity resistive wall on MHD stability in the tokamak and RFP.

In the tokamak the major disruption is generally preceeded by a period of magnetic oscillations with a poloidal number, m = 2 and a toroidal mode number, n = 1 [1]. These (2,1) magnetic oscillations are generally interpreted as arising from resistive tearing modes [2,3] and probe measurements have shown this to be so experimentally [4]. Major disruptions generally either occur as the result of a density limit [5] or a current limit (usually at a limiter safety factor $q_\psi \sim 2$) [6]. A feature of the large amplitude m=2 activity, for current limit disruptions in JET, is the general absence of rotation [7] of the (2,1) magnetic activity. This absence of rotation and the hard disruptive limit for $q_\psi \sim 2$ has been shown to be consistent with the effects of a resistive wall on m=2 MHD instabilities in Ref [8]. In Section 3.1 we examine from a linear viewpoint the stabilising effect of mode rotation on resistive wall instabilities. In particular we show that both analytically and computationally that a locked ideal (2,1) mode occurs for $q_\psi < 2$; this result is in agreement with the calculations in Ref [8].

In larger tokamaks the (2,1) predisruptive activity is generally observed to lock in a particular phase after a period of initial rotation. This mode locking which can occur for any value of q_ψ (not just $q_\psi \sim 2$) has been observed for example in JET [7] and DIIID [9]. Rutherford [10], and Nave and Wesson [11], have proposed analytic and semi-analytic models to explain this mode locking phenomenon. They postulate that the mode locking arises because of a net torque on the plasma which is due to the eddy currents driven in the resistive wall by the rotating mode. In Section 4.1 we shall show that full numerical solutions of the tokamak reduced MHD equations are in good agreement with the analytic theory of Rutherford [10]. These results are also in accord with numerical mode locking simulations by Persson and Bondeson [8,12].

In the RFP consideration of the effects of a resistive wall can markedly change the stability boundaries, relative to those obtained

with a perfectly conducting wall. In the limit of an ideal wall several authors have produced RFP profiles, with realistic zero current conditions at the wall, which are stable to all resistive and ideal MHD instabilities at zero β [13,14]. However, when the effects of a resistive wall are considered these profiles are always unstable to ideal non-resonant instabilities. In addition a broad range of m=0 and m=$\pm$1 resonant tearing modes are destabilised by considering the effects of a resistive wall. These tearing modes can be stabilised by rotating the plasma sufficiently fast, but the ideal resistive-wall instabilities remain essentially unaffected by rotation. In Section 3.2 we will present numerical and analytic results which confirm the destabilising effect of a resistive wall for the MHD stable profiles (with an ideal wall) of Antoni et al [14]. In a previous publication [15] we have presented results on the resistive wall instabilities which occur for tearing mode stable profiles of the type parameterised by Robinson [13]. The torque effect due to the eddy currents in the resistive wall, which acts to inhibit mode rotation in the tokamak, is also present in the RFP. Due to the different geometry and generally larger fluctuation level in the RFP the rotation damping time due to the resistive wall is considerably shorter than that in the tokamak. These results are discussed in Section 4.2.

In Section 2 we describe the MHD equations and numerical methods which are used in these studies. In Sections 3 and 4 linear and non-linear results are presented on the influence of a resistive wall on MHD instabilities. Finally, conclusions are given in Section 5.

2. Equations and Numerics

For reasons of computational efficiency we solve a set of reduced equations, derived by Strauss, which are applicable to RFP geometries [16]. These equations are based on an ordering scheme in which the fluctuating magnetic field is assumed to be small relative to an axisymmetric mean average field, and slowly varying on an Alfvenic time scale. In addition the pressure is ordered to be small and cylindrical geometry is assumed, so that toroidal effects are ignored. The ordering and derivation of these reduced equations is discussed fully in Ref [16]; we state the results here without a detailed derivation.

The magnetic field ($\vec{B}$) is split into a spatial average ($\langle\vec{B}\rangle$) and fluctuating ($\tilde{\vec{B}}$) part

$$\vec{B} = \langle\vec{B}\rangle + \tilde{\vec{B}} \qquad (1)$$

where

$$\langle\vec{B}\rangle = (2\pi L)^{-1}\int_o^L dz \int_o^{2\pi} \vec{B} d\theta \qquad (2)$$

and L is the periodicity length in the azimuthal direction (z). The fluctuating magnetic field and velocity are represented in a potential form,

$$\tilde{\vec{B}} = \vec{\nabla}\times(\psi\langle\vec{B}\rangle + \alpha\vec{r}) \qquad (3)$$

and

$$\tilde{\vec{V}} = \langle\vec{B}\rangle \times \vec{\nabla}\phi/|\langle B\rangle|^2 \qquad (4)$$

where $\vec{r}$ is the unit radial vector. The parallel component of Ohms law yields

$$\frac{\partial\psi}{\partial t} = -\frac{\vec{B}}{|\langle\vec{B}\rangle|^2}\cdot\nabla\psi + \frac{\eta}{S}\vec{C} \qquad (5)$$

where

$$\vec{C} = \frac{1}{|\langle\vec{B}\rangle|^2}\nabla\cdot(|\langle\vec{B}\rangle|^2\nabla\psi - \langle\vec{B}\rangle\langle\vec{B}\rangle\cdot\nabla\psi - \vec{r}\langle\vec{B}\rangle\cdot\nabla\alpha) \qquad (6)$$

Here the magnetic field is normalised to the equilibrium toroidal magnetic field, B_o, at r = 0, distance is normalised to the minor radius 'a', the resistivity (η) is normalised to its value at r = 0, time is normalised to the Alfven time $\tau_A = a\sqrt{(\mu_o\rho_o)}/B_o$ (with ρ_o the density at r = 0), and $S = \tau_R/\tau_A$ where $\tau_R = a^2\mu_o/\eta_o$ is the resistive transit time. An equation for α is derived from $\vec{J}\times\langle\vec{B}\rangle + \langle\vec{J}\rangle\times\tilde{\vec{B}} = \vec{0}$ (a consequence of the ordering)

$$\left(\frac{1}{r^2}\frac{\partial^2}{\partial\theta^2} + \epsilon^2\frac{\partial}{\partial\xi^2}\right)\alpha = \langle\vec{B}\rangle\cdot\nabla\frac{\partial\psi}{\partial r} \qquad (7)$$

where $\epsilon = 2\pi a/L$ is the effective inverse aspect ratio and $\xi(= 2\pi Z/L)$ is the 'toroidal' angle ($0 \le \xi \le 2\pi$). The evolution of ϕ arises from the vorticity equation

$$\frac{\partial}{\partial t}(\nabla^2\phi) + \nabla\cdot(\vec{V}\nabla^2\phi + \nabla\{\frac{|\vec{V}|^2}{2}\}\times\langle\vec{B}\rangle) = \vec{B}\cdot\nabla\frac{\langle\vec{B}\rangle\cdot\langle\vec{J}\rangle}{|\langle B\rangle|^2} - \vec{B}\cdot\nabla\left(\frac{\vec{C}}{\vec{B}\cdot\nabla\vec{C}}\right) \qquad (8)$$

These equations have been used by Holmes et al [17] for a study of tearing modes in the RFP; the notation and conventions in this paper are identical to those of Ref [17]. In addition to Eqns (3) to (8) for the fluctuating field, $\tilde{\vec{B}}$, equations for the evolution of the average magnetic field $\langle\vec{B}\rangle$ may also be derived. These are given in Refs [16] and [17] and will not be reproduced here.

The effects of the resistive wall are manifest in the boundary conditions. Using the so called thin wall approximation [18], that the wall resistive skin depth >> wall thickness, yields

$$[\tilde{b}_r]_{r_-}^{r_+} = 0 \tag{9}$$

$$[\frac{\partial r\tilde{b}_r}{\partial r}]_{r_-}^{r_+} = \tau_W \frac{\partial \tilde{b}_r}{\partial t} \tag{10}$$

where r_+, r_- are just inside and outside the resistive wall respectively and the wall time constant $\tau_W = \tau_A^{-1} a\delta/\eta_w$, with δ being the wall thickness and η_w its resistivity. Taking the wall to be at r=1, representing the field in the vacuum region outside the wall in terms of modified Bessel functions as

$$\tilde{B}_r = AK_m'(\epsilon nr) \tag{11}$$

where primes denote derivatives with respect to r and using conditions (9) and (10) gives:

$$\frac{\partial}{\partial r} r\tilde{B}_r - (m^2 + n^2\epsilon^2)K_m/\frac{dK_m}{dr}\tilde{B}_r = -\tau_W \frac{\partial \tilde{B}_r}{\partial t} \tag{12}$$

For the velocity boundary condition we use $\tilde{V}_r = 0$ at r = 1. This leads to the problem that we form a resistive boundary layer near the wall [19] since for $V_r = 0$ Ohm's law becomes $\partial\tilde{B}_r/\partial t = \eta/S\ (\nabla^2\tilde{\vec{B}})_r$ (and $\partial\tilde{B}_r/\partial t \neq 0$ at r = 1 for a resistive wall). This $\tilde{V}_r = 0$ boundary layer however has no effect on the marginal stability and in general has little effect on the overall stability. The remaining boundary conditions at r = 0 for ψ and ϕ arise from regularity of the solution.

Of particular interest for the resistive wall stability problem is the issue of the effects of plasma rotation. To bring out the main features of this effect we will consider the simplest form of rotation - uniform toroidal rotation. It is in fact simpler and equivalent to

translate the wall toroidally, which represents a Doppler shift of the time derivatives. So for example boundary condition (12) becomes

$$\frac{\partial r\tilde{B}_r}{\partial r} - (m^2 + n^2\epsilon^2)\, K_m / \frac{dK_m}{dr}\, \tilde{B}_r = -\tau_W \left(\frac{\partial \tilde{B}_r}{\partial t} + i\omega_W \tilde{B}_r\right) \qquad (13)$$

where ω_W is the angular frequency of the 'rotating' wall.

In the numerical solution of Eqs (5) to (8) we use a finite difference representation in the radial direction (r) and a truncated Fourier series in the angular directions θ, ξ. Thus for example ψ is represented as

$$\psi(r,\theta,\xi,t) = \sum_{m,n} \left(\psi^s_{m,n}(r,t)\, \sin(m\theta+n\xi) + \psi^c_{m,n}(r,t)\, \cos(m\theta+n\xi)\right) \qquad (14)$$

The linear terms of Eqs (5) to (8) are time advanced fully implicitly using a time centred difference scheme. This allows very rapid convergence to the linear eigenvalues [20]. For non-linear calculations the additional terms are included purely explicitly and the timestep is limited accordingly when the non-linear terms become dominant.

Although we have emphasised the applicability of these reduced equations to the RFP they may also be applied to the tokamak. In fact in the tokamak limit $\langle B_\xi \rangle \sim 1$ and $\langle B_\theta \rangle \sim o(\epsilon)$ they reduce to the familiar reduced tokamak equations [21]. Numerically for tokamak problems we solve the reduced tokamak equations:-

$$\frac{\partial \psi}{\partial t} = \left(\frac{1}{r}\frac{\partial \psi}{\partial \theta}\frac{\partial}{\partial r} - \frac{\partial \psi}{\partial r}\frac{1}{r}\frac{\partial}{\partial \theta}\right)\phi + \epsilon \frac{\partial \phi}{\partial \xi} + \frac{\eta \nabla^2_\perp \psi}{S} \qquad (15)$$

$$\frac{\partial \nabla^2_\perp \phi}{\partial t} + \left(\frac{1}{r}\frac{\partial \phi}{\partial \theta}\frac{\partial}{\partial r} - \frac{\partial \phi}{\partial r}\frac{1}{r}\frac{\partial}{\partial \theta}\right) \nabla^2_\perp \phi =$$

$$\left(\frac{1}{r}\frac{\partial \psi}{\partial \theta}\frac{\partial}{\partial r} - \frac{\partial \psi}{\partial r}\frac{1}{r}\frac{\partial}{\partial \theta}\right) \nabla^2_\perp \psi + \frac{\partial \nabla^2_\perp \psi}{\partial \xi} \qquad (16)$$

Using the appropriate limit of Eqn (12) as the wall boundary condition. It should be noted that there is no distinction between fluctuating and average quantities here, and these equations are also used to evaluate the average fields ($\langle\psi\rangle$ and $\langle\phi\rangle$). These reduced equations are solved for tokamak problems because they contain fewer terms and are thus more efficient computationally than the reduced RFP equations.

We will not examine how good an approximation the reduced tokamak and RFP equations are to the full MHD equations in this paper. In Ref [22] it is shown that the reduced tokamak equations are a good approximation at large aspect ratio and low β, and in Ref [17] it is shown that the reduced RFP equations are a good approximation to the full MHD equations when $\beta=0$. In fact the reduced RFP equations contain an exact representation of the marginal ideal MHD equations and thus the marginal ideal and resistive stability boundaries are reproduced exactly by these equations.

3. Linear Results

3.1 Tokamak

Considering a resonant surface of radius, r_s, where the safety factor $q(r_s) = m/n$ we may derive an approximate dispersion relation for the (m, n) resistive wall tearing mode. Assuming a vacuum to exist for $r_s \leq r \leq r_w$ (with r_w being the wall radius) we may solve in this region to obtain $\psi = AI_m(\epsilon nr/r_w) + BK_m(\epsilon nr/r_w)$, where I_m and K_m are the modified Bessel functions. In the tokamak limit the arguments of the Bessel functions are small ($\epsilon nr/r_w << 1$) and the first term in the series expansion of I_m, K_m is sufficient. We retain the full terms I_m, K_m however so that the results may be latter applied to the RFP. The approximation of a vacuum for $r_s \leq r \leq r_w$ is often quite good for the (2,1) tearing mode since in many cases there may be little toroidal current flowing outside the q = 2 surface. Using boundary condition (12) we find that

$$\lim_{\lambda\to 0} \left[\frac{1}{\psi}\frac{d\psi}{dr}\right]_{r_s-\lambda}^{r_s+\lambda} = \Delta'$$

$$= \Delta'_v + \frac{\alpha(r_s)\,(K'_m(\epsilon n))^2\,\omega\tau_w}{r_s K'_m(\epsilon n\bar{r}_s)[\omega\tau_w K'_m(\epsilon n)\beta - K'_m(\epsilon n\bar{r}_s)\alpha(r_w)]} \qquad (17)$$

where $\alpha(r) = (m^2/r^2 + n^2\epsilon^2/r_w^2)$, $\beta = K'_m(\epsilon n\bar{r}_s)I'_m(\epsilon n) - K'_m(\epsilon n)I'_m(\epsilon n\bar{r}_s)$, $\bar{r}_s = r_s/r_w$, and Δ'_v is the value of Δ' with no wall (i.e. $\tau_w = 0$). In this equation and throughout the rest of the paper we have reverted to a dimensional form. In the tokamak limit ($n\epsilon<<1$) Eq (17) may be considerably simplified to the result obtained previously [10]

$$\Delta' = \Delta'_v - \frac{2m\omega\tau_w \bar{r}_s^{-2m-1}}{r_w[\omega\tau_w(1-\bar{r}_s^{-2m})+2m]} = \Delta'_v - \frac{\omega\tau_w(\Delta'_v - \Delta'_w)}{\omega\tau_w + 2\,m(1-\bar{r}_s^{-2m})^{-1}} \qquad (18)$$

where Δ'_w is the value Δ' when $\tau_w = \infty$.

The logarithmic discontinuity (Δ') is related to the growth rate, ω, by [23]

$$\tau_A \omega = 0.547 \, (r_w \Delta')^{4/5} \, (\frac{\eta}{S})^{3/5} \, \left| \frac{n\epsilon q' \langle B_z \rangle r_w}{q B_o} \right|^{2/5} \qquad (19)$$

and thus the requirement for instability ($\omega>0$) is that $\Delta'>0$. In fact from Eqns (18) and (19) we may prove the more general result that when $\Delta'_v > 0$, then instability exists for all τ_w (except possibly $\tau_w=\infty$). This result was noted previously by Jensen and Chu [24], and is the analogue of that proved by Pfirsch and Tasso in the ideal limit [25]. It is most easily seen by regarding Eqs (18) and (19) as describing two curves in the (Δ',ω) plane; the intersection(s) of these curves describe the solution(s) of the problem. Equation (19) is a curve $\omega \alpha \Delta'^{4/5}$ in the $\omega>0$, $\Delta'>0$ quadrant while Eqn (18) varies between Δ'_v for $\omega = 0$ and a smaller value as $\omega \to \infty$. Thus if $\Delta'_v>0$ the two curves must intersect in the $\omega>0$, $\Delta'>0$ quadrant and hence a growing solution ($\omega>0$) exists for any τ_w as noted above. This is a very useful result since it shows that to examine the ideal and resistive stability boundaries, with a resistive wall ($0 \le \tau_w < \infty$), it is sufficient to study the stability boundaries with no wall ($\tau_w = 0$). We have numerically confirmed the result that $\Delta'_v>0$ implies instability for all τ_w in many cases. An example is shown in Fig 1 where the variation of growth rate (ω) with τ_w for the profile $q = 1.1 \, (1 + 25r^8)^{1/4}$ with $\epsilon = 0.1$, $m = 2$, $n = 1$, $\eta \equiv 1$, and $S = 10^7$. The open circles shown in Fig 1 are from the numerical solution of the reduced tokamak equations and the solid line is from the dispersion relation [Eqns (18) and (19)]; they are in good agreement. In this case $\Delta'_v = 4.6$ while with a perfectly conducting wall ($\tau_w=\infty$), $\Delta'_w = -1.68$. Hence although instability persists for all finite τ_w the singular limit $\tau_w = \infty$ is stable; this stability for $\tau_w = \infty$ is also confirmed by the numerical solution of the reduced tokamak equations.

The resistive wall stability is modified significantly by plasma rotation [18]. For the simple uniform toroidal rotation discussed in Section 2 the effect is to Doppler shift the growth rates in the wall boundary conditions by $i\omega_w$. So for example the dispersion relation for the resistive wall tearing mode [Eq (18)] becomes [10]

$$\Delta' = \Delta'_v - \frac{2m(\omega + i\omega_w)\tau_w \bar{r}_s^{-2m-1}}{[(\omega + i\omega_w)\tau_w(1-\bar{r}_s^{2m}) + 2m]r_w} \qquad (20)$$

It should be noted however that we must not Doppler shift the growth rate (ω) in the resistive layer relation, Eq (19). With the rotation ($\omega_w \neq 0$) the growth rate is complex and the proof that the resistive wall tearing mode is unstable for all τ_w, if $\Delta'_v > 0$, is no longer valid. If $\Delta'_v \geq \Delta'_w \geq 0$ then as $\omega_w \to \infty$ in Eq (20)

$$\Delta' = \Delta'_v + \frac{2m\bar{r}_s^{2m-1}}{[\bar{r}_s^{2m}-1]r_w} = \Delta'_w \qquad (21)$$

Hence as the rotation speed is increased the growth rate asymptotes to the ideal wall ($\tau_w = \infty$) growth rate. For the case that $\Delta'_v > 0 > \Delta'_w$ it may be shown that a critical rotation frequency (ω_{crit}) exists beyond which the mode is stabilised [8,18]. These results on the stabilising effects of rotation are reproduced by numerical solutions of the reduced tokamak equations. Figure 2 shows a comparison of the dispersion relation [Eqs (19) and (20)] with numerical growth rate (ω_R) and frequency (ω_I) for the profile $q = 1.1\ (1 + 54r^8)^{1/4}$, with $S = 5 \times 10^5$, $\epsilon = 0.1$, $m = 2$ and $n = 1$. For this profile $\Delta'_v = 5.3$ and $\Delta'_w = 2.6$ and so the result given in Eq (21) is applicable with the growth rate asymptoting to the ideal wall growth rate at high rotation speed.

The rotation effects described above are for a resonant tearing mode. Non resonant ideal modes may be destabilised by resistive wall effects. The growth rate for these non-resonant modes is given by [18]

$$\omega\tau_w = r_w\Delta'_1 \qquad (22)$$

with

$$\Delta'_1 = \lim_{\lambda \to 0} \left[\frac{1}{\psi}\frac{d\psi}{dr}\right]_{r_w-\lambda}^{r_w+\lambda} \qquad (23)$$

A particular case of such an ideal mode is that which occurs for $q_a < 2$ in the tokamak [8]. Rotation has essentially no effect on these ideal modes. The appropriate dispersion relation is obtained by Doppler shifting the growth rate in Eq (22) by $i\omega_w$ [18].

This result is also confirmed in our numerical simulations though the numerical technique shows poor convergence to a linear eigenvalue for $\omega_w > \omega_R$. Figure 3 shows how the ideal growth rate ($S = \infty$) varies with ω_w for $q_a = 1.7$ with $J_z \alpha (1-r^2)$, $\tau_w = 10^4$ and $\epsilon = 0.1$. It can be seen that ω_R is essentially independent of ω_w while $\omega_I = -\omega_w$; in agreement with the analytic results. These locked modes for $q_\psi < 2$ are thought to be associated with the hard disruption limit which occurs in the tokamak [8]. In JET for example when $q_\psi \to 2$ a disruption occurs which is proceeded by a (2,1) mode with a growth time of the order of the wall time constant [7]. Also this mode often shows no coherent oscillations and is essentially locked to the wall throughout most of its duration [7]; this is in contrast to density limit disruptions (with $q_\psi > 2$) where the pre-disruption (2,1) [or (3,1)] activity generally has a long oscillating (non-locked) phase [7].

3.2 RFP

In the RFP a wider range of instabilities are destabilised by a finite conductivity wall, than in the tokamak. With a perfectly conducting wall it is possible to find RFP equilibria which are stable to all ideal and resistive modes at $\beta = 0$ [13,14]. Here we will adopt the equilibrium parameterisation given Ref [14]. The equilibria in this case are specified by $\langle \vec{J} \rangle \times \langle \vec{B} \rangle = 0$ and

$$\mu \equiv \frac{\langle \vec{J} \rangle \cdot \langle \vec{B} \rangle}{|\langle \vec{B} \rangle|^2} = \mu_c (1-r^\alpha) \tag{24}$$

Figure 4(a) shows Δ' for this profile with $\mu_c = 3.6$ and $\alpha = 3.2$. Here Δ' is defined as

$$\Delta' = \lim_{\lambda \to o} \left[\frac{1}{\tilde{B}_r} \frac{d\tilde{B}_r}{dr} \right]_{r_s - \lambda}^{r_s + \lambda} \tag{25}$$

[this is consistent with the tokamak definition Eq (17)].
Results are shown in Fig 4(a) for a vacuum ($\tau_w = 0$) and ideal wall ($\tau_w = \infty$) at $r = 1$. The convention is used that the modes which are resonant within the field reversal surface have toroidal mode numbers

$n<0$. With an ideal wall for this profile ($\mu_c = 3.6$, $\alpha = 3.2$) all modes are stable (i.e. have $\Delta' < 0$) but with a vacuum wall a wide range of $m = 0$ and 1 modes are destabilised. Recalling that $\Delta'_v > 0$ implies instability for all $\tau_w (\neq \infty)$ we see that the resistive wall will destabilise a wide range of tearing modes. Figure 4(b) shows the growth rates obtained by solving the reduced pinch equations for the $m = 0$ and $m = 1$ ($n<0$) modes with $S = 4 \times 10^5$, $\epsilon = 0.1$ and $\tau_w = 10^3$. The regions of instability correspond to $\Delta'_v > 0$; as $n\epsilon \to 0$ the $m = 0$ growth rate tends to zero since $\omega \alpha (n\epsilon)^{2/5}$ [see Eq (19)]. For $-1.8 < n\epsilon < -1.6$ Fig 4(b) shows instability (see also Fig 5). These are non-resonant 'on-axis' ideal modes [18] and are analogous to the $q_a < 2$ ideal tokamak modes discussed in Section 3.1. To study non-resonant ideal modes in the RFP we define a generalisation of Eq (23).

$$\Delta'_1 = \lim_{\lambda \to o} \left[\frac{1}{\tilde{B}_r} \frac{d\tilde{B}_r}{dr} \right]_{r_w + \lambda} \qquad (26)$$

where $\tilde{B}_r$ is obtained by solving the marginal force balance equation [RHS of Eq (8)]. The growth rates of the ideal non-resonant modes are then given by Eq(22).

Figure 5 shows Δ'_1 as a function of $n\epsilon$ for equilibria defined by Eq (24) with various values μ_c and α; with a superconducting wall these equilibria are stable to all resistive and ideal modes. However with a resistive wall ideal instability ($\Delta'_1 > 0$) occurs for non resonant modes 'within the axis' ($n<0$) and 'outside the wall' ($n>0$). For typical RFP parameters ($\mu_c \sim 3.4$) the internal and external non-resonant modes are about equally important. At higher μ_c (and F, θ_o) the external modes become more important, and vice-versa at lower μ_c. These results are in accord with those given in Refs [26,27]. Figure 6 shows a comparison of the numerical growth rate obtained by solving the reduced pinch equations with the result from dispersion relation Eq (22) with $\mu_c = 3.4$, $\alpha = 3.5$, $S = \infty$, $\tau_w = 10^3$ and $-1.7 \leq n\epsilon \leq -1.2$. There is excellent agreement between the numerical solution and dispersion relation.

The effects of rotation on resistive wall instabilities are the same in the RFP as the tokamak; the resistive wall tearing modes are stabilised by rotation if $\Delta'_w < 0$, while for sub-Alfvenic rotation the non-resonant ideal modes remain locked and essentially unaffected by the rotation [18]. These conclusions are confirmed in Fig 7 which shows the growth rate as a function of rotation frequency (ω_w) for $\mu = 3.6\,(1 - r^{3.2})$ with $S = 5 \times 10^4$, $\epsilon = 0.1$, and $\tau_w = 10^3$. There are

two pairs of growth rate curves shown, one for n = 18 and the other for n = 20. The n = 20 case is a resonant tearing mode with $\Delta'_w = -1.67$; the strong stabilisation effect for $\omega_w \gtrsim 5 \times 10^{-3}\ \tau_A^{-1}$ can be seen. In contrast the n = 18 case is the on-axis ideal non-resonant mode; its growth rate (ω_R) increases very slightly with ω_w, a result predicted analytically when the inertia is retained [18], while its frequency (ω_I) is such that it remains locked in the laboratory frame ($\omega_I \simeq -\omega_w$).

If we examine the stability to ideal non resonant modes, for profiles which are unstable to internal tearing modes but stable to ideal modes with a perfectly conducting wall, then we find that the internal on-axis ideal mode is strongly unstable. Figure 8 shows Δ'_1 for the internal non resonant modes with the profile $\mu = 3.5\ (1 - r^{2.8})$; this profile is ideally stable but tearing mode unstable with a superconducting wall. In Fig 8 results are shown for various locations (R_{wall}) of a superconducting wall in the vacuum region. The results show that the ideal on-axis mode is unstable, even if there is an infinitely conducting wall just outside a resistive liner, for this tearing mode unstable profile. This situation may correspond to the HBTX-1B RFP experiment where there was a resistive liner at r = 26.7 cm and thick (effectively infinitely) conducting shell at r = 28.8 cm. In this experiment large amplitude locked modes, resonant near the magnetic axis, were sometimes observed [28]. In these cases the usual internal resonant magnetic activity is also present; indicating perhaps that the profiles are tearing mode unstable. Thus it appears that the ideal on-axis resistive wall modes may provide an explanation for the experimentally observed locked modes.

4. Nonlinear Results

4.1 Tokamak

The linear and non-linear results are in many ways analogous. In the absence of plasma rotation the ability of the tearing mode to grow sufficiently slowly that its flux can penetrate the resistive wall gives the linear result quoted in Section 3.1, that a tearing mode is unstable for all τ_w ($\neq\infty$) if it is unstable for $\tau_w = 0$. Non-linearly we have an analogous result that the saturation width is relatively independent of τ_w, for $\tau_w < \infty$. Figure 9 shows the m/n = 2 single helicity island width (W) evolution for various τ_w with $q = 1.1\ (1 + (r/0.627)^4)^{1/2}$, $S = 10^5$ and $\epsilon = 0.1$. From this figure it can be seen that the island saturation widths for $\tau_w = 0$ and ∞ differ considerably. The saturation widths for $\tau_w = 0$ and 10^4 however differ very little, despite a 40% reduction in linear growth rate for the $\tau_w = 10^4$ case, relative to $\tau_w = 0$.

Rotation also has an analogous effect in the linear and non-linear regimes. In Section 3.1 it was shown that the linear growth rate asymptotes to the $\tau_w = \infty$ result as $\omega_w \to \infty$ for all $\tau_w > 0$. The non-linear analog of this result is that the saturation width asymptotes to the $\tau_w = \infty$ result as $\omega_w \to \infty$. Figure 10 shows this for the same parameters as Fig 9; it can be seen with a sufficiently fast rotation ($\omega_w = 0.06$) that the $\tau_w = 10^3$ (2,1) single helicity island evolution is essentially identical to the $\tau_w = \infty$ result. This is despite the large difference in growth rates and saturation widths in the absence of rotation between the $\tau_w = 10^3$ and ∞ cases (Fig 9).

Linearly we have seen that rotating the plasma causes the tearing mode to rotate (and not remain locked to the wall). However non-linearly a mechanism exists which tends to cause the tearing mode to lock [10,11]. This arises because the eddy currents driven in the resistive wall by the rotating mode produce a net torque which opposes and reduces the plasma rotation. We may calculate this torque by integrating the poloidal and toroidal components of the equation of motion over the plasma volume

$$\int_o^{r_w} \rho r^2 \frac{d\langle V_\theta \rangle}{dt}\, dr = \frac{r_w^2}{2\mu_o} \sum_{(m,n)} \left(\tilde{B}_{r_{m,n}} \tilde{B}_{\theta_{m,n}} \right)_{r = r_w} \tag{27}$$

and

$$\int_o^{r_w} \rho r \frac{d\langle V_z \rangle}{dt}\, dr = \frac{r_w}{2\mu_o} \sum_{(m,n)} \left(\tilde{B}_{r_{m,n}} \tilde{B}_{z_{m,n}} \right)_{r = r_w} \tag{28}$$

We consider the case in which a single Fourier component (m,n) is dominant and eliminate $\tilde{B}_\theta$, $\tilde{B}_z$ in Eqns (27) and (28) using the resistive wall boundary conditions. The result for the rate of change of rotation frequency (Ω) is

$$\tau_A^2 \frac{d\Omega}{dt} = \frac{-\Omega \tau_w}{\bar{r}_s} \frac{r_w \tilde{B}_r^2}{2WB_o^2} \frac{m^2/\bar{r}_s^2 + n^2\epsilon^2}{m^2 + n^2\epsilon^2} \tag{29}$$

where we have assumed that the average flows ($\langle V_\theta \rangle, \langle V_z \rangle$) exist only within the island and considered the plasma as a solid body rotator (ie the entire plasma has the same angular frequency). We relate $\tilde{B}_r$ ($r = r_w$) to the island width W by assuming a vacuum to exist for $r_s < r < r_w$. With this assumption we find

$$\tau_A^2 \frac{d\Omega}{dt} = -\left(\frac{W}{8r_s}\right)^3 r_w^2 \left(\frac{mB_\theta q'}{qB_o}\right)^2 \frac{2r_s(\Delta_v' - \Delta_w')\, m\Omega\tau_w}{4(m^2+n^2\epsilon^2)/A + m^2A\Omega^2\tau_w^2/(m^2+n^2\epsilon^2)} \quad (30)$$

where

$$A = \frac{2\, K_m'(\epsilon n) r_w^2}{m\, K_m'(\epsilon n r_s)} \left(K_m'(\epsilon n) I_m'(\epsilon \bar{r}_s) - I_m'(\epsilon n) K_m'(\epsilon \bar{r}_s)\right) \quad (31)$$

and $\frac{B_\theta q'}{q}$ is evaluated at r_s.

In the tokamak limit ($n\epsilon \ll 1$), A=1 and Eq (30) reduces to

$$\tau_A^2 \frac{d\Omega}{dt} = -\left(\frac{W}{8r_s}\right)^3 r_w^2 \left(\frac{mB_\theta q'}{qB_o}\right)^2 \frac{2r_s m\Omega\tau_w(\Delta_v'-\Delta_w')}{4m^2 + \Omega^2\tau_w^2} \quad (32)$$

which is the result given in Ref [10]. In deriving these equations for $d\Omega/dt$ we have used a simple MHD model and have taken no account of viscosity or neo-classical effects. The effect of viscosity would be to couple the flow in the island region to the plasma outside the island, thus increasing the volume of angular momentum which the torque has to slow. The effect of neo-classical terms is to damp poloidal rotation in the tokamak [29], and thus weaken the torque effect from the resistive wall. These effects must be borne in mind when comparing this theory with experiment. The analytic expressions, Eqs (30) and (32), are however the appropriate formulae to compare with numerical solutions of the reduced tokamak equations. Figure 11 shows the time evolution of Ω and $d\Omega^2/dt$, for the same equilibrium as Fig 9, and compares the analytic [Eq (32)] and numerical results. For this case the imposed plasma rotation frequency $\omega_w = 10^{-2}$, $S = 10^6$, and $\tau_w = 400$. From Fig 11 it can be seen that the analytic theory gives a reasonable approximation for the time evolution of $d\Omega^2/dt$. The solutions of Eq (32) for Ω are discussed in Ref 11.

For $\Omega\tau_w \ll m$

$$\Omega = \Omega_o e^{-(C\tau_w t/4m^2\tau_A^2)} \quad (33)$$

where $\Omega_o = \Omega(t = 0)$,

$$C = \left(\frac{W}{8r_s}\right)^3 r_w^2 \left(\frac{mB_\theta q'}{qB_o}\right)^2 2\, r_s m\, (\Delta_v' - \Delta_w')$$

and we have assumed W is constant in time. It should be noted that since the decay (in Eqn (33)) is exponential, true mode lock ($\Omega = 0$) never occurs within the limitations of this theory. It is also interesting to note that these expressions for mode lock depend on the Alfvenic timescales and are independent of the resistive timescale (τ_R). This is in contrast to the non-linear growth time of the tearing mode which varies with τ_R and determines the duration of the pre-disruption MHD activity. Thus given that the Alfven time is relatively invariant between tokamaks, we see that the ratio of disruption duration (τ_R timescale) to mode lock time (τ_A timescale) is greater in the larger tokamaks. Hence mode lock is more likely to occur in large high temperature tokamaks (e.g. JET) than in their smaller counterparts. An alternate way of seeing this result is to examine the island width required to produce mode lock. Solving Eq (32) we find that the island width (W_c) to reduce an initial frequency (Ω_o) by a factor of 10 in a mode growth time is,

$$W_c^3 = C_1 \epsilon^{-2} \gamma \tau_A^2 (0.99 \Omega_o^2 \tau_w + 36.8/\tau_w) \qquad (34)$$

where $C_1 = 256\, q^4 m^{-3}\, r_s^{-2}\, q'^{-2} (\Delta'_v - \Delta'_w)^{-1}$, and γ is the growth rate of the perturbed magnetic field. Taking typical values we find $W_c \sim 10\%$ for JET, $\sim 25\%$ for DITE [30], and $\sim 70\%$ for TOSCA [31]. Thus mode lock is likely to occur in JET but unlikely to occur in TOSCA, where W_c exceeds the disruption threshold. As noted above however care must be exercised in applying Eq (32) directly to the experiment and these values for W_c are most appropriately interpreted as a relative scaling between the various experiments.

4. RFP Results

In the RFP a full non linear study would necessarily include a self consistent dynamo model. Here we focus on the very restricted problem of the mode locking for a single helicity mode.

Considering a typical internally resonant mode m = 1, n = -11 for the profile $\mu = 3.6\,(1 - r^{2.9})$ with $\epsilon = 0.2$, we find evaluating the constants in Eq (30) that

$$\tau_A^2 \frac{d\Omega}{dt} = \frac{9 \times 10^{-2} W^3 \Omega \tau_w}{(10.2 + 0.39\, \Omega^2 \tau_w^2) r_w^3} \qquad (35)$$

Comparing with the equivalent result for a typical m = 2, n =1 mode in the tokamak shows that the RFP mode lock rates are ~ 8 times faster than in the tokamak when $\Omega\tau_w \ll 1$, and ~ 12 times faster when $\Omega\tau_w \gg 1$. The main

reason for the higher mode lock rates in the RFP is that the factor $(\Delta_v'-\Delta_w')$ occurring in Eq (30) is $\sim$5 times larger in the RFP than in the tokamak. This difference in $(\Delta_v'-\Delta_w')$ between the RFP and tokamak is a fairly general result and occurs because the wall has a strong stabilising influence for the RFP, but does not in general for the tokamak; thus we should expect rapid mode lock in the RFP. Also in the RFP a broad range of internally resonant modes with relatively large fluctuations ($\delta B/B \sim 1\%$) are generally observed [32], thus further enhancing the mode lock rates in the RFP relative to the tokamak. An exception is near $q_\psi \sim 2$ in the tokamak where $(\Delta_v'-\Delta_w')$ becomes large and calculations show rapid mode lock [8].

These results on mode lock in the RFP are again borne out by the numerical calculations. Figure 12 shows the time variation of Ω and $d\Omega^2/dt$ for the single helicity m/n = 1/11 with $\mu = 3.6\ (1-r^{2\cdot 9})$. The solid curve for $d\Omega^2/dt$, in Fig 15, comes from evaluating the analytic result, Eq (30); it can be seen that there is reasonable agreement between the analytic and numerical results for the time variation of $d\Omega^2/dt$.

5. Conclusions

It has been shown that allowing for the effects of a resistive wall can destabilise ideal and resistive MHD instabilities, which would be stable if the wall were perfectly conducting. Near $q_\psi \sim 2$ for some tokamak configurations, and in general in the RFP, an ideal resistive-wall mode occurs with a growth time $\alpha 1/\tau_w$. The analytic and numerical studies presented show that these ideal resistive-wall modes are essentially unaffected by sub-Alfvenic plasma rotation and remain locked to the wall. They appear likely candidates for explaining the $q_\psi=2$ disruption activity in the tokamak [8], the observed locked modes in HBTX1B [28] and much of the MHD activity in HBTX1C [33].

For the resistive-wall tearing modes, sufficiently high plasma rotation velocities are stabilising if $\Delta_w'<0$, and modes do not lock to the wall. There is however a non-linear effect which causes mode lock [10,11]; the eddy currents driven in the wall by the rotating MHD activity produce a net torque on the plasma which opposes, and slows, the plasma rotation. Full non-linear calculations, which are in reasonable agreement with analytic theory, have shown this mode locking effect in both the RFP and tokamak. In general the mode lock rates predicted by the theory are faster in the RFP than in the tokamak. This is mainly due to the generally large values of $(\Delta_v'-\Delta_w')$ in the RFP. Strictly the theory predicts an exponential decay of Ω as the mode locks and exact mode lock (Ω=0) never occurs. However the exponential decay does

rapidly cause the mode rotation time to exceed the disruption duration, and thereby produce effective mode lock. Also in this region of slow rotation any small stray error fields may lead to absolute mode lock [34].

References

[1] McGuire, K. M, Robinson, D. C., Phys Rev Lett 44 (1980) 1666.

[2] Carreras, B. A., Hicks, H. R., Holmes, J. A., Waddell, B. V., Phys Fluids 23 (1980) 1811.

[3] Wesson, J. A., Sykes, A., Turner, M. F., Plasma Physics and Controlled Fusion Research (Proc 10th Int. Conf. London 1984) 1 (1985) 28.

[4] Robinson, D. C., Phil Trans. R. Soc. A 300 (1981) 525.

[5] Axon K. B., Clark W. H. M., Cordey J. G. et al, in Plasma Physics and Controlled Nuclear Fusion Research 1980 (Proc 8th Int. Conf. Brussels 1980) Vol 1. IAEA Vienna., (1981) 413.

[6] Robinson, D. C., Todd, T. N., Plasma Phys. and Contr. Fusion 28 (1986) 1177.

[7] Snipes, J. A., Nucl Fusion 28 (1988) 1085 and Campbell, D. J., Duperrex, P. A., et al, Plasma Physics and Contolled Fusion Research 1987 (Proc 11th Int. Conf. Kyoto 1986) 1 IAEA Vienna (1987) 433.

[8] Bondeson, A. and Persson, M., Nucl. Fusion 28 (1988) 1887.

[9] Kellman, A. G., Bull of Am. Phys. Soc. 32 (1987) 1846.

[10] Rutherford, P. H., 'Resistive Instabilities in Tokamaks', Princeton Lab. Report PPL-2277 (1985).

[11] Nave, M. F. F., Wesson, J. A., in Controlled Fusion and Plasma Physics 1987 (proc. 13th European Conf. Madrid, 1987), Vol 3, European Physical Society, (1987) 1103.

[12] Persson, M., and Bondeson, A., in Theory of Fusion Plasmas (Proc. Workshop Varenna 1987) Editrice Composition; Bologna, 1988, 325.

[13] Robinson, D. C., Nucl. Fus. 18 (1978) 939.

[14] Antoni, V., Merlin, D., Ortolani, S., Paccagnella, R., Nucl. Fus. 26 (1986) 1711.

[15] Hender, T.C., Gimblett, C. G., Robinson, D. C., in Controlled Fusion and Plasma Heating (Proc. 13th European Conf., 1986) Vol. I, European Physical Society (1986) 61.

[16] Strauss, H. R., Phys. Fluids 27 (1984) 2580.

[17] Holmes, H. A., Carreras, B. A., Diamond, P. H., Lynch, V. E., Phys. Fluids 31 (1488) 1166.

[18] Gimblett, C. G., Nucl. Fusion 26 (1986) 617.

[19] Gimblett, C G 'Plasma Instabilities caused by a finitely conducting wall' Proc of "Physics of Mirrors, Reversed Field Pinches and Compact Tori", Varenna, Vol. I (1987) 241.

[20] Charlton, L. A., Holmes, J. A., Hicks, H. R., Lynch, V. E., Carreras, B. A., J Comput. Phys. 63 (1986) 107.

[21] Strauss, H. R., Phys. Fluids 20 (1977) 1354.

[22] Holmes, J. A., Carreras, B. A., Hender, T. C., Hicks, H. R., Lynch, V. E., Masden, B. F., Phys. Fluids 26 (1983) 2564.

[23] Coppi, B., Greene, J. M., Johnson, J. L., Nucl. Fus. 6 (1966) 101.

[24] Jensen, T. H. and Chu, M. S., J. Plasma Phys. 30 (1983) 57.

[25] Pfirsch, P., Tasso, M., Nucl. Fusion 11 (1979) 259.

[26] Ho, Y. L. and Prager, S. C. Phys. Fluids 31 (1988) 1673.

[27] Miller, G. Phys. Fluids B, 1 (1989) 387.

[28] Cunnane, J. A., Evans, D. E., Gimblett, C. G., Hender, T. C., Tsui, H. Y. W., 'Coherent flucutations in HBTXIB RFP', Proc. of "Physics and Compact Tori" Varenna, Vol III, (1987) 1017.

[29] Hirshman, S. P., and Sigmar, D. J., Nucl. Fusion 21 (1981) 1079.

[30] Paul, J. W. M., Axon, K. B., Burt J., et al, in Plasma Physics and Controlled Nuclear Fusion Research, 1976 (Proc. 6th Int. Conf. Berchtesgaden 1976) Vol 2. IAEA Vienna (1977) 269.

[31] Cima, G., Robinson, D. C., Thomas C. L., Wotton, A. J., in Plasma Physics and Controlled Nuclear Fusion Research, 1976 (Proc. 6th Int. Conf. Berchtesgaden 1976) Vol 1. IAEA Vienna (1977) 335.

[32] Brotherton-Ratcliffe, D., Gimblett, C. G., Hutchinson, I. H., Plasma Phys. and Contr. Fusion 29 (1987) 161.

[33] Alper, B., Bevir, M. K., Bodin, H. A. B., et al, Plasma Phys. and Contr. Fusion 31 (1989) 205.

[34] Hender, T. C., Gimblett, C. G., Robinson, D. C., Proc. of 14th European Conf. on Controlled Fusion and Plasma Heating, Dubrovnik Vol. 1, (1988) 205.

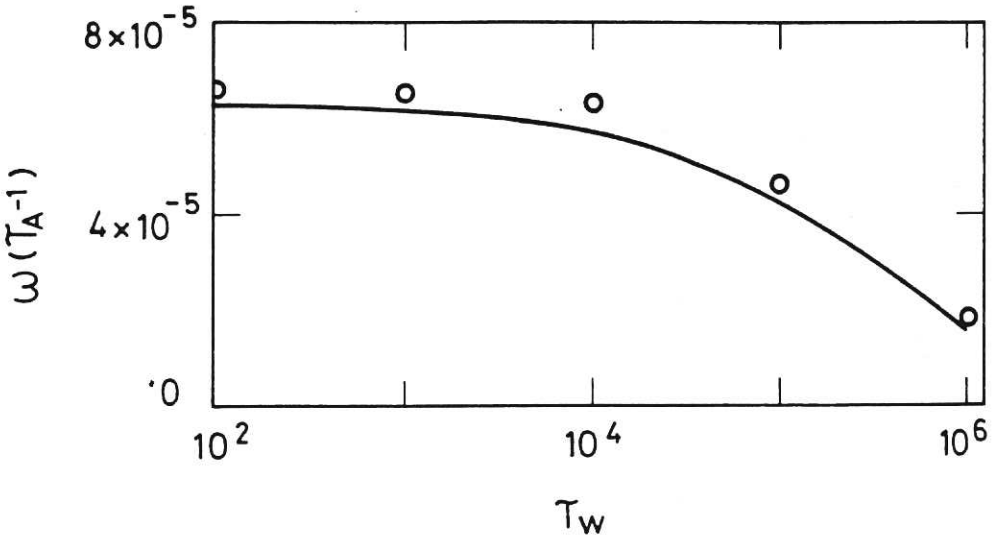

Fig. 1 Comparison of growth rate versus τ_w between dispersion relation (solid line) and numerical results (circles) for $m=2$, $n=1$ with $q=1.1\ (1+25r^8)^{1/4}$ and $S=10^7$.

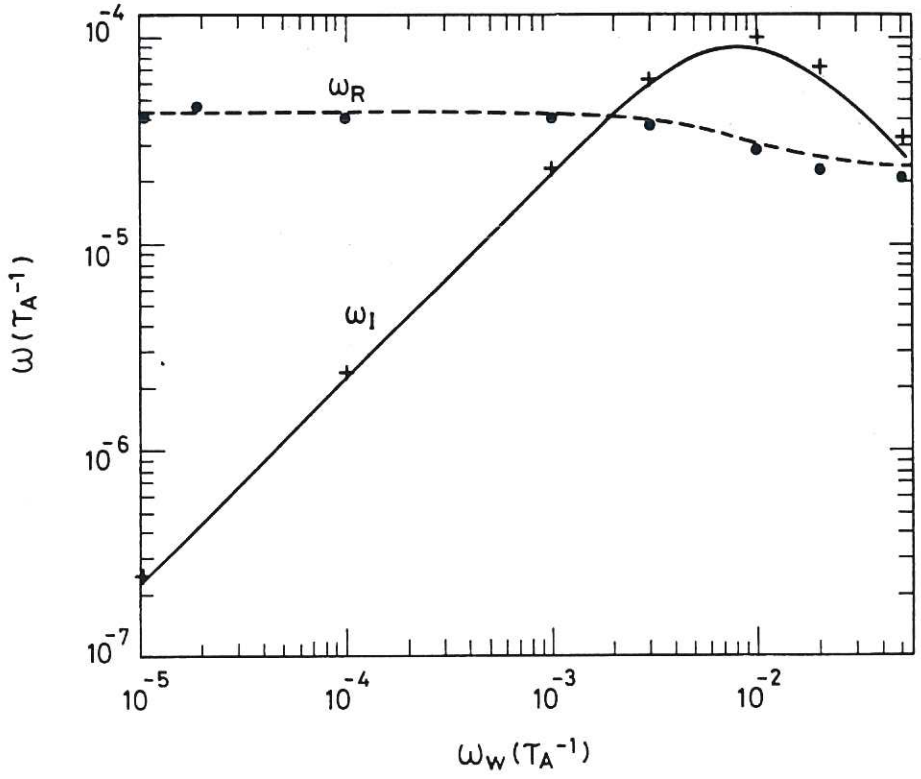

Fig. 2 $m=2$, $n=1$ growth rate (ω_R) and frequencies (ω_I) versus rotation frequency (ω_w) from the dispersion relation (solid and broken curves) and numerical calculations (dots and pluses) for $S=5\times10^5$ and $\epsilon=0.1$.

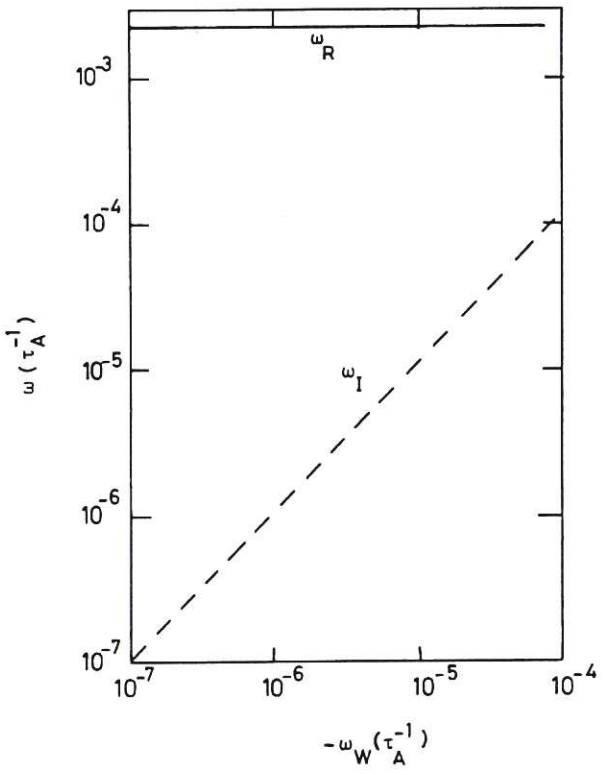

Fig. 3 Numerical growth rate and frequency of the ideal $m=2$ mode ($q_a=1.7$) showing mode lock ($\omega_I \approx -\omega_W$).

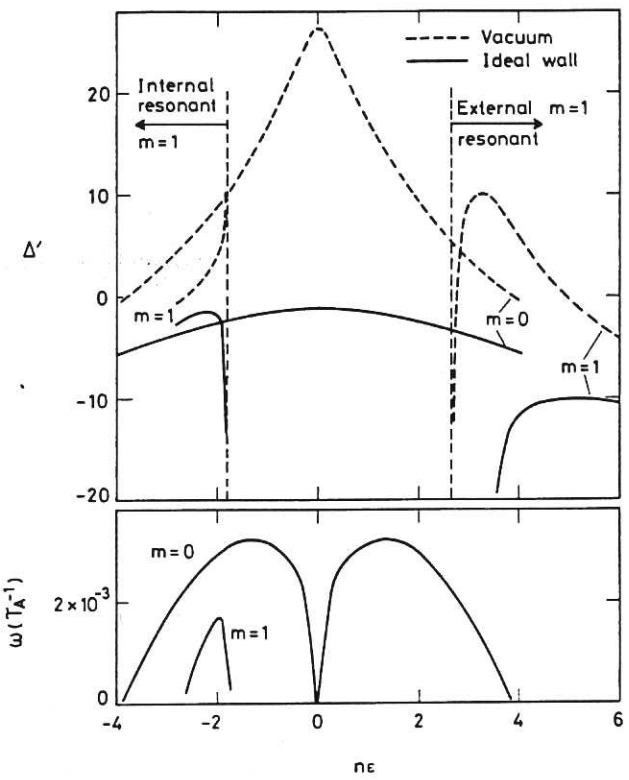

Fig. 4 Δ' and growth rate (ω) as a function of toroidal wavelength ($n\epsilon$) for RFP profile $\mu=3.6\,(1-r^{3.2})$. Δ' results (upper plot) are shown with (solid curve) and without (broken curve) a wall. Growth rates (lower plot) are for $\tau_w=10^3$ and $S=4\times10^5$.

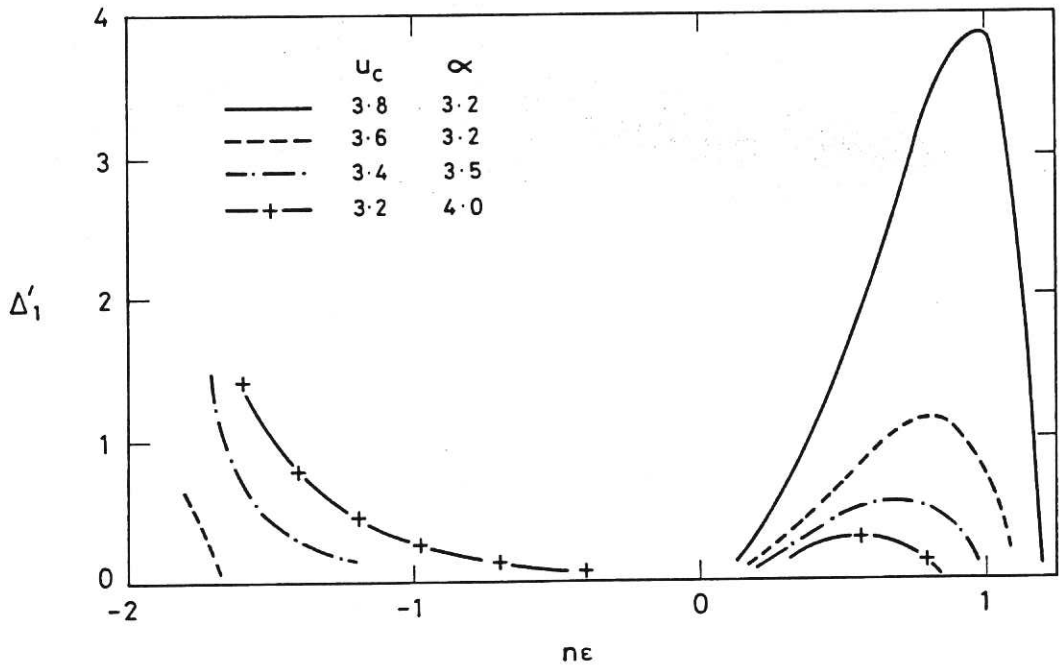

Fig. 5 Internal and External non-resonant Δ_1' values for various μ_c, $\alpha\,[\mu=\mu_c(1-r^{\alpha})]$.

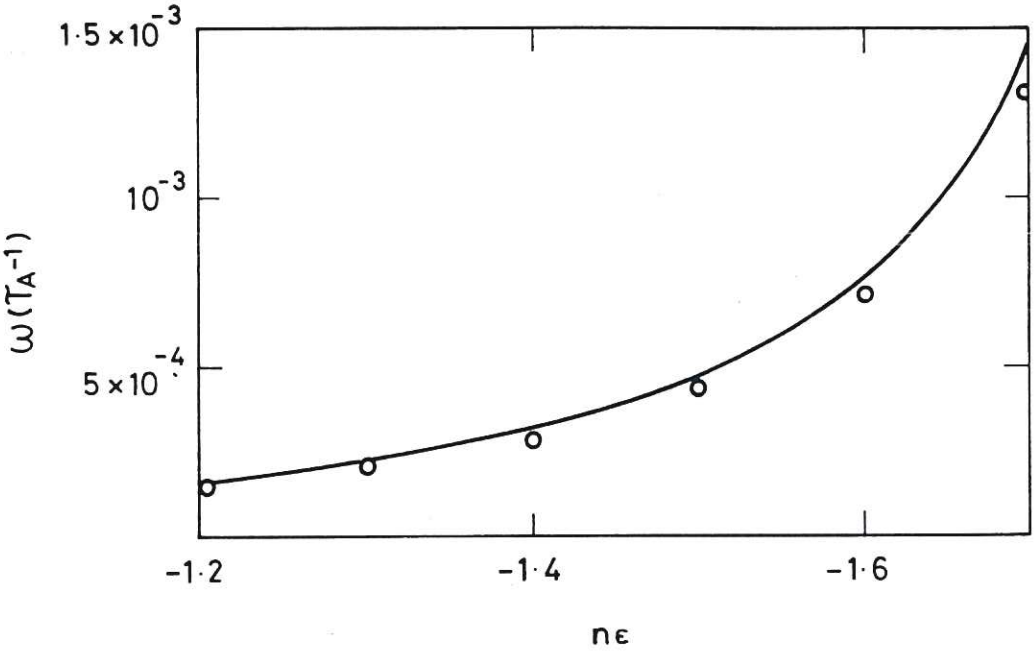

Fig. 6 Growth rate of the internally non-resonant $m=1$ ideal modes v $n\epsilon$ for $\mu=3.4(1-r^{3.5})$ and $\tau_w=10^3$. Results are shown from the dispersion relation (solid line) and from the numerical calculations (circles).

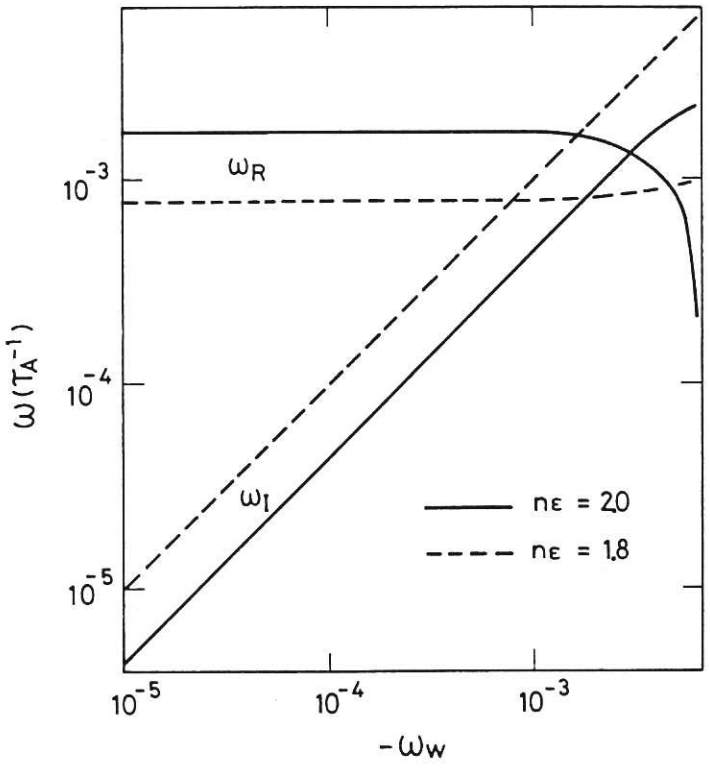

Fig. 7 Growth rate (ω_R) and frequency (ω_I) as a function of rotation frequency (ω_w) for $\mu=3.6\,(1-r^{3.2})$, $S=5\times10^4$ and $\tau_w=10^3$. For the non-resonant ideal mode ($n\epsilon=1.8$) there is a slight destabilisation but the resonant tearing mode ($n\epsilon=2.0$) is strongly stabilised for $|\omega_w|>5\times10^{-3}$.

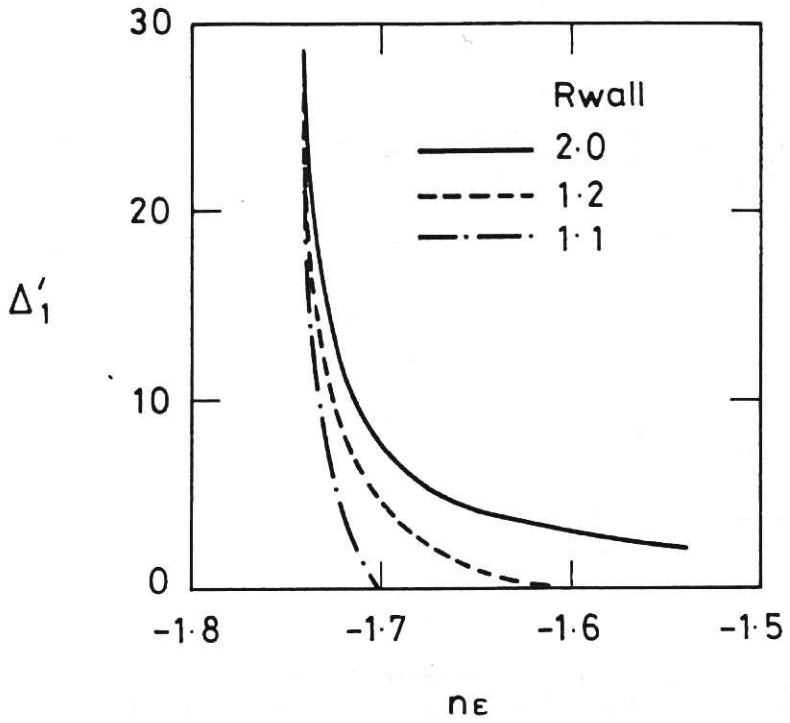

Fig. 8 Non resonant Δ_1' values versus $n\epsilon$ for $m=1$, $\mu=3.5\,(1-r^{2.8})$ and various ideal wall locations (R_{wall}).

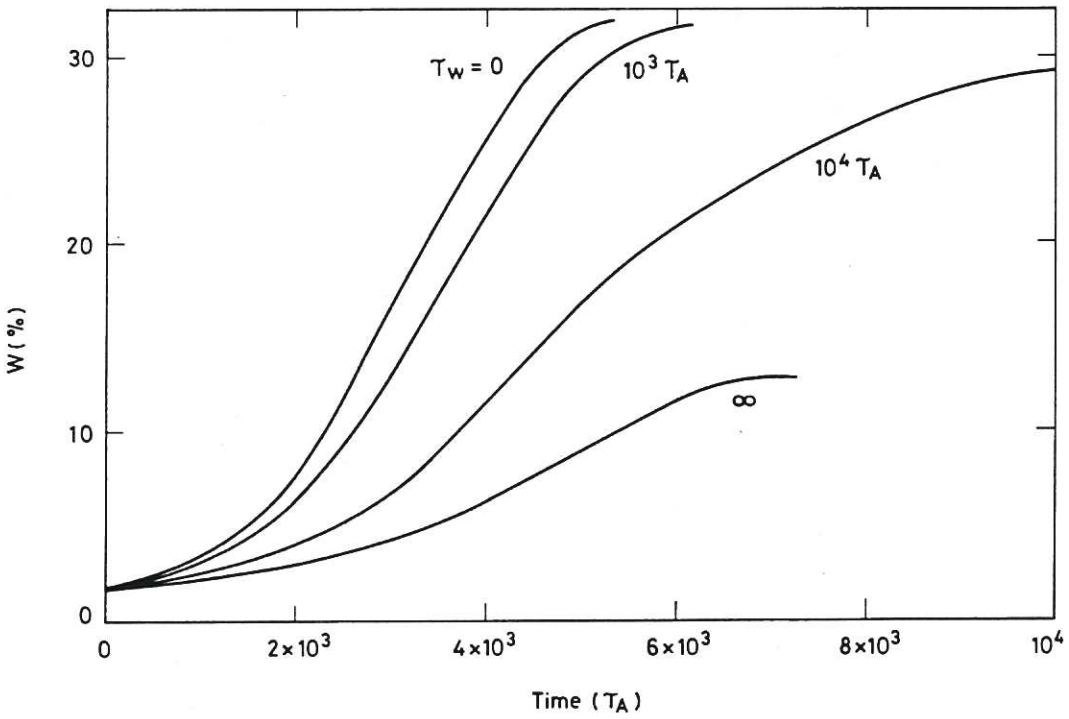

Fig. 9 Single helicity $m/n=2/1$ non-linear island width evolution for various τ_w with $q_a=3$ and $S=10^5$.

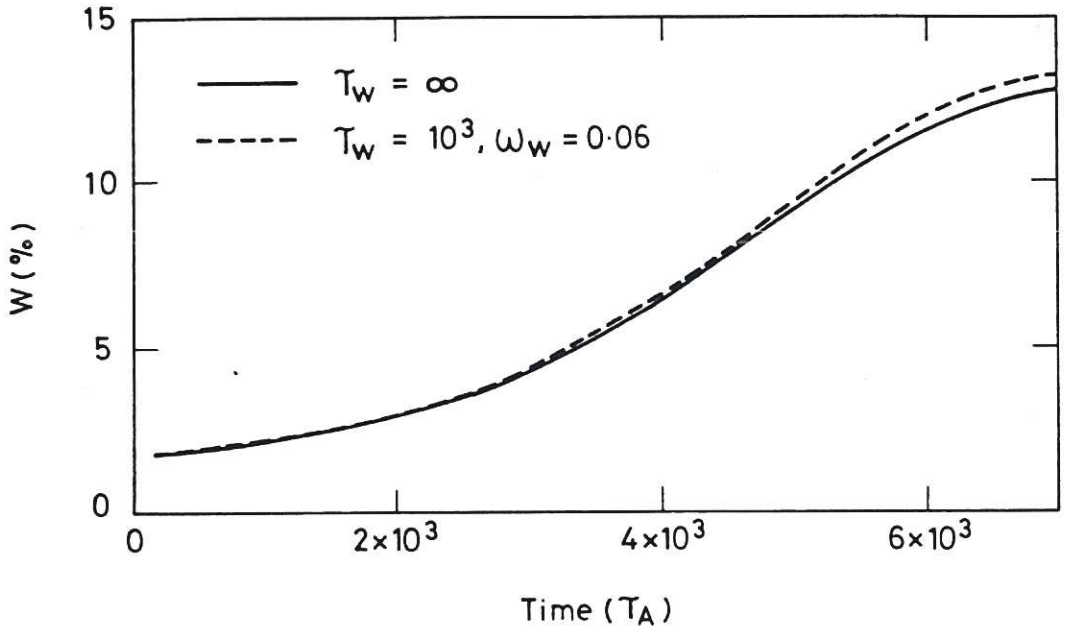

Fig. 10 Single helicity $m/n=2/1$ non-linear island width evolution showing strong rotation ($\omega_w=0.06$) causes the resistive wall mode to saturate to the ideal wall ($\tau_w=\infty$) width.

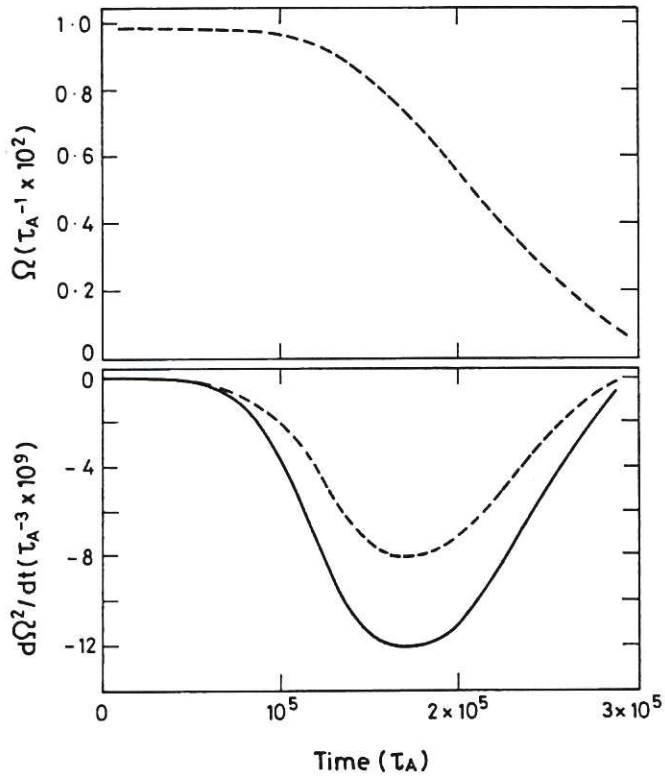

Fig. 11 Non-linear evolution of Ω and $d\Omega^2/dt$ for a single helicity $m/n=2/1$ simulation with $S=10^6$ and $q_a=3$. In the lower plot the numerical (broken curve) and analytic Eq(32) (solid curve) results are compared.

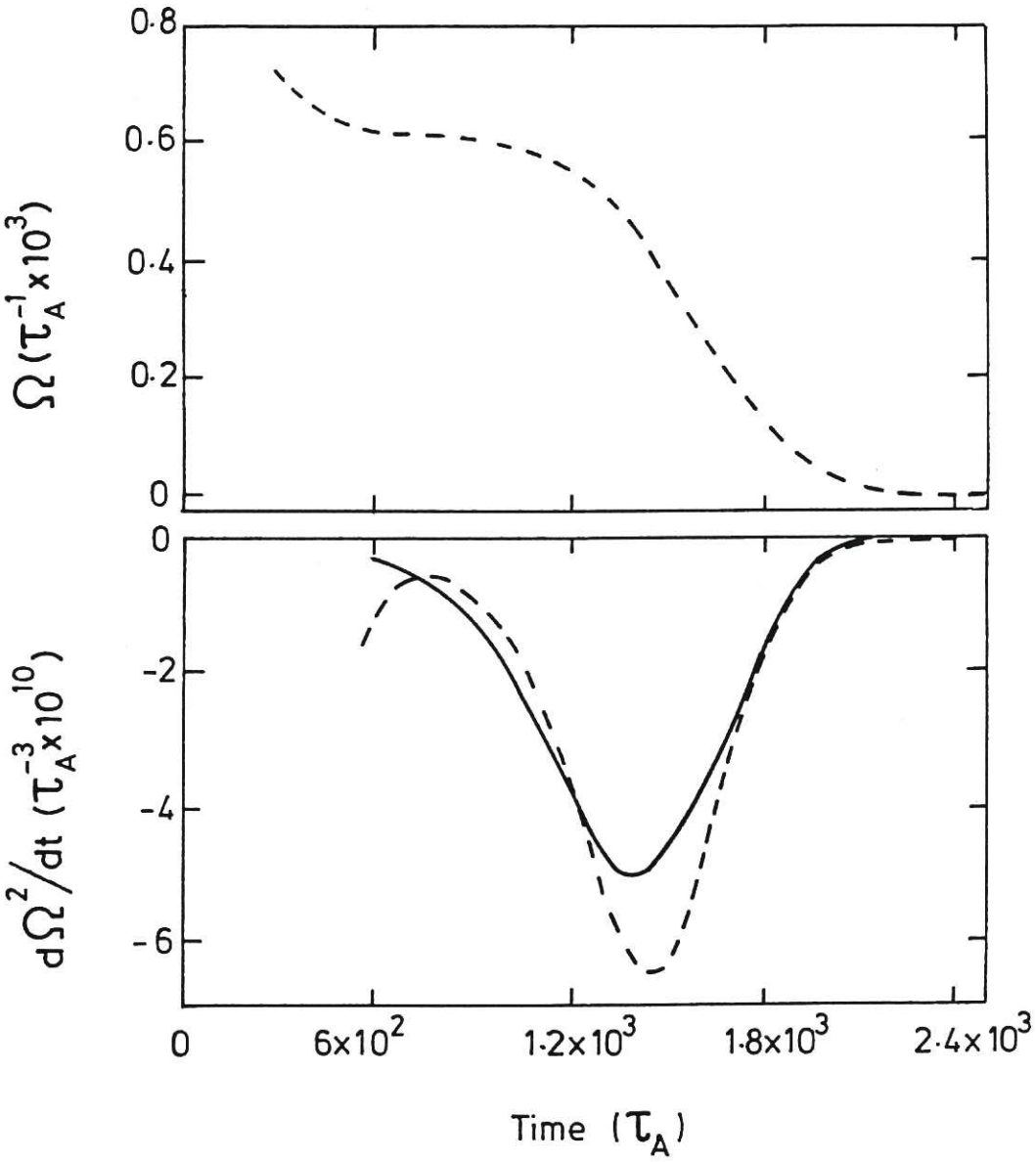

Fig. 12 As Fig. 11 but for the RFP profile $\mu=3.6\ (1-r^{2.9})$ with the single helicity $m/n=-1/11$. The analytic result (solid curve, lower plot) is from Eq(30).